JOURNAL OF APPLIED CRYSTALLOGRAPHY

Volume 50 (2017)

Supporting information for article:

ECCI, EBSD and EPSC Characterization of Rhombohedral Twinning in Polycrystalline α-Alumina Deformed in the D-DIA Apparatus

Shirin Kaboli and Pamela C. Burnley

Supplementary Materials

ECCI, EBSD and EPSC Characterization of Rhombohedral Twinning in Polycrystalline α-Alumina Deformed in the D-DIA Apparatus

Shirin Kaboli and Pamela C. Burnley

Department of Geoscience and High Pressure Science and Engineering Center

University of Nevada Las Vegas (UNLV), Las Vegas, NV, United States

Keywords: Rhombohedral twin, ECCI, EBSD, EPSC

EXPERIMETNAL

D-DIA Experiments

The alumina piston, in series with the sample, was wrapped in a 25 μm thick nickel metal jacket and placed at the center of the sample assembly. A crushable alumina piston was used at one end of the assembly to transfer the load from the tungsten carbide anvils to the sample. For experiment MgGe_003, a W3%Re–W25%Re thermocouple was placed at the top end of the sample. No thermocouple was used for experiment FOR_99. The temperature of the hot spot for each experiment was derived from the calibration of temperature as a function of the furnace power using the kinetics of MgO + Al_2O_3 reaction (Watson et al., 2002) as described in (Kaboli & Burnley, 2017). The alumina piston is about 1 mm away from the hot spot in the sample assembly. Therefore the temperature for the alumina (as reported in Table 1 in the text) was determined by assuming that the pressure within the sample and the piston is the same. The equation of state of alumina (Fei, 1995; d'Amour et al., 1978) was then used to solve for the temperature in the alumina that would produce the observed d-spacing at the experimental pressure.

For experiment MgGe_003, an initial annealing step was performed at ~988 ºC. The first deformation sequence was performed at ~692 ºC followed by second deformation sequence at ~807 ºC. For experiment FOR_99, the initial annealing step was performed at ~1243 ºC followed by deformation at ~1110 ºC. Deformation was conducted at a constant strain rate of ~10^{-5} s^{-1}. During the compression experiments diffraction data was collected as a group of five X-ray spectra, each for a duration of 60 seconds, from the alumina piston and then the sample. Radiographic images were collected in between the groups of spectra. For d-spacing analysis the

5 groups of 60 second spectra were summed to create 300 second spectra. The diffracted X-rays were collected with 9 energy-dispersive detectors arranged in a semi-circle centered around the transmitted beam, each measuring a full powder pattern from the sample. In this study, the diffraction data from the two detectors in the compression direction and one transverse detector was analyzed. At the final macroscopic strain, the D-DIA motors were stopped, the temperature was quenched, and then the experiment was decompressed.

Analysis of Alumina X-ray Spectra

For experiment MgGe_003, the bulk modulus for germanate spinel (Mg_2GeO_4) was used (Weidner & Hamaya 1983) and for experiment FOR_99, the bulk modulus for forsterite olivine (Mg_2SiO_4) was used (Kudoh & Takeuchi, 1985). Thermal expansion coefficients of germanate spinel were found in (Ross & Navrotsky, 1987) and thermal expansion coefficients of forsterite olivine were found in (Hazen, 1976) and thermal expansion coefficients of alumina were found in (Alderbert & Traverse, 1984). For experiment MgGe_003, the hydrostatic pressure was ~4.48 and ~4.60 GPa for first and second deformation sequences, respectively, and for experiment FOR_99, the hydrostatic pressure was ~7.36 GPa.

Elastic Plastic Self-Consistent (EPSC) Modeling

The stress supported by alumina pistons for the two experiments was derived by comparing the experimental diffraction data from the D-DIA experiments with the simulated diffraction data from the EPSC models. An executable FORTRAN EPSC code (EPSC3) provided by C. Tome (Tome & Oliver, 2002) (as modified and used by (Burnley, 2015)). Each EPSC model consisted of an aggregate of 49108 grains evenly distributed through the Euler space. The unit cell parameters and single-crystal isothermal elastic constants *Cij* for EPSC models of alumina were

calculated for the temperature and pressure conditions for each experiment. The adiabatic *Cij* was first calculated as the second order Taylor expansion at constant pressure (Anderson & Isaak 1995). The values for first and second order temperature and pressure derivatives of alumina from (Goto *et al.*, 1989) were used. The adiabatic *Cij* was then converted to the isothermal *Cij* by means of its thermodynamic equivalent (Anderson & Isaak, 1995).

For experiment MgGe_003, the deformation of the alumina in the first sequence of the experiment was modeled using basal, prismatic and pyramidal slip systems and rhombohedral twinning system. The lattice strains for six diffraction peaks observed in the experimental diffraction spectra were modeled including (104), (110), (113), (024), (116), and (214). Models were run at a constant strain rate up to a maximum of 8% sample strain over 900 displacement increments and under a uniaxial strain boundary condition. The CRSS and hardening parameters for the slip and twinning systems were adjusted so that the numerical diffraction data from alumina EPSC models closely matched the experimental diffraction data from the D-DIA experiment. In the second sequence of experiment MgGe_003, alumina deformed elastically while the germanate spinel sample deformed plastically. Therefore, plastic deformation in the alumina sample belongs to the first deformation sequence of experiment MgGe_003. For experiment FOR_99, macroscopic strain measurements were not possible since radiographic images were unavailable. Thus, the macroscopic stress was estimated by comparing the maximum observed lattice strain for the average of lattice strain of all reflections with those obtained from an EPSC model in which only elastic deformation was considered.

Sample Preparation

The deformed samples from the D-DIA experiments were cold mounted in epoxy and cut along a plane parallel to the compression direction. The grinding and polishing were carried out manually on spinning wheels at a 150 rpm rotation speed. Grinding was performed with #600, #800, #1000, #1200 silicon carbide papers. Polishing was performed with 6, 3, 1 and 0.4 μm particle size diamond suspensions with yellow DP-lubricant on MD-Chem, MD-Mol, and MD-Nap polishing cloths until a scratch-free surface was observed using an optical microscope. Water was used as a lubricant during grinding and polishing. The samples were rinsed with water between each grinding and polishing step. Between each polishing step, the samples were ultrasonically cleaned in distilled water for 10 minutes and dried completely in air. Sample surfaces were final polished with a 0.05 μm colloidal silica suspension using a VibroMet vibratory polisher. In order to remove damaged surface layers caused by the cold-working effects of grinding and polishing, the samples were etched with a 10% hydrochloric acid solution for a few minutes, rinsed immediately with distilled water, ultrasonically cleaned for 30 minutes and air dried completely. No coating was applied to sample surfaces prior to imaging at low beam energy in SEM but the samples were carbon coated prior to imaging and EBSD at high beam energy in SEM using an EMS 150T carbon coater.

Mechanical testing	Pressure/load	Temperature[1] (ºC)	Strain rate (s^{-1})	Deformation mode	Reference[2]
Compression in Griggs apparatus	0.5-1.5 GPa	20-950	2×10^{-5}	Prismatic slip	(Castaing *et al.*, 1981)
Compression	Ambient	800-1300	2×10^{-5}	Basal slip and rhombohedral twinning	(Castaing *et al.*, 2002)
Compression in Griggs apparatus	1.5 GPa	400-700	10^{-5}	Basal slip and basal and rhombohedral twinning	(Castaing *et al.*, 2004)
Compression in Griggs apparatus	1.5 GPa	600-1000	2×10^{-5}	Prism slip and rhombohedral twinning	(Korinek & Castaing, 2003)
Compression in Griggs apparatus	1.5 GPa	800	2×10^{-5}	Dislocation slip and basal and rhombohedral twinning	(Geipel *et al.*, 1994)
Compression in Griggs apparatus	1.5 GPa	200-950	2×10^{-5}	Prism slip at 200 ºC and Basal slip at 400 ºC	(Lagerlöf et al., 1994)
Compression in Griggs apparatus	1.5 GPa	600-1000	2×10^{-5}	Dislocation slip	(Castaing *et al.*, 2000)
Compression in Instron universal testing machine	500 g	< 1100	10^{-6}	Rhombohedral twinning	(Choi & Auh, 1995a; 1995b)
Compression in Instron testing machine	-	1400 - 1600	$1.2 \times 10^{-5} – 8.3 \times 10^{-4}$	Grain boundary sliding	(Ishihara *et al.*, 1999)
Compressive creep	Ambient	1400-1700	-	Basal slip and rhombohedral twinning	(Bertolotti & Scott, 1971)
Compression	500 Kg	350-1100	8.7×10^{-6} - 8.7×10^{-4}	Rhombohedral twinning	(Scott & Orr, 1983)
Compression	Ambient	1100-1500	10^{-5} - 10^{-2}	Rhombohedral twinning	(Stofel & Conrad, 1963)
Compression in D-DIA apparatus	3.9-5.5 GPa	1400	4.8×10^{-5}	Dislocation slip[4]	(Raterron *et al.*, 2013)
Indention	20, 50, 100 g	RT	-	Dislocation slip and rhombohedral and basal twinning	(Hockey, 1971)
Indentation	6N	RT	-	Dislocation slip and rhombohedral twining	(Zarudi *et al.*, 1996)
Indentation	0.1-0.25 N	RT	-	Pyramidal slip and basal twinning	(Chan & Lawn, 1988)
Shock	13-26 GPa	400[3]	-	Dislocation slip and twinning	(Beauchamp *et al.*, 1985)
Shock	6 and 7.8 GPa	-	-	Dislocation slip and basal twinning	(Chen *et al.*, 2006)
Shock	6.5 and 12 GPa	-	-	Dislocation slip	(Mukhopadhyay *et al.*, 2012)
Shock	(0.6 Kg) 5.88 N	-	$>10^4$	Dislocation slip	(Wade *et al.*, 2016)
Shock	23 GPa	RT	-	Dislocation slip	(Merala *et al.*, 1988)
Shock	0.1-86 MN	-	-	Dislocation slip and twining	(Dancer *et al.*, 2011)
Shock via laser irradiation	-	-	long pulse (2.2 us)	Basal and rhombohedral twinning	(Luo *et al.*, 2007)
Shock	5, 12, 23 GPa	RT	-	Prismatic slip and Basal twinning	(Wang & Mikkola, 1992)
Shock	-	RT	18 km/s	Rhombohedral twining	(Zhang *et al.*, 2008)

Mechanical testing	Pressure/load	Temperature[1] (ºC)	Strain rate (s^{-1})	Deformation mode	Reference[2]
Four-point bending	-	-196-1200	-	Rhombohedral twinning below 1000 ºC and basal twinning above 1000 ºC	(Heuer, 1966)
Four-point bending	1.4-310 MPa	1200-1750	10^{-6} - 10^{-4}	Basal slip and grain-boundary sliding	(Heuer *et al.*, 1980)
Four-point bending	100-2000 psi	1600-1800	2×10^{-7} - 2×10^{-5}	Dislocation slip	(Warshaw & Norton, 1962)
Four-point bending	1.4-310 MPa	1200-1750	10^{-6} - 10^{-4}	Diffiusional creep	(Cannon *et al.*, 1980)
Four point bending	44 and 36 MPa	1400	10^{-6} - 10^{-3}	Grain boundary sliding	(Chokshi, 1990)
Bending, creep in tension, and torsion about c-axis	-	1500	-	Dislocation glide and climb	(Barber & Tighe, 1965)

Table S1. Summary of plastic deformation experiments on alumina under a variety of experimental conditions

Notes:
[1] RT: room temperature
[2] Starting material differed in grain size, orientation and single versus polycrystallinity in listed references
[3]Maximum adiabatic temperature rise
[4] Based on EPSC models

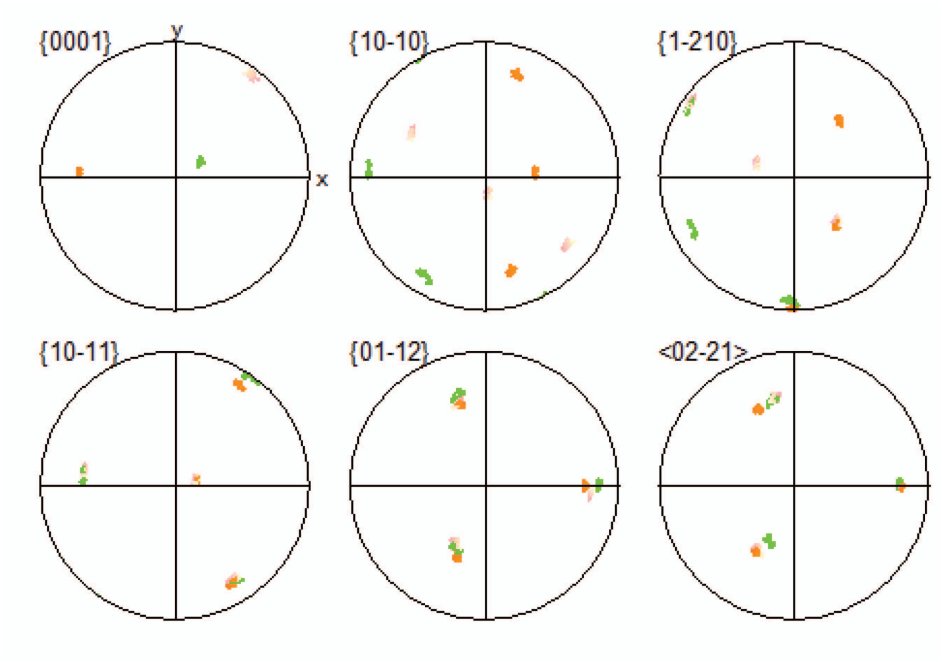

Figure S1. Raw pole figures obtained from EBSD crystal orientation mapping corresponding to Figure 8 in the text.

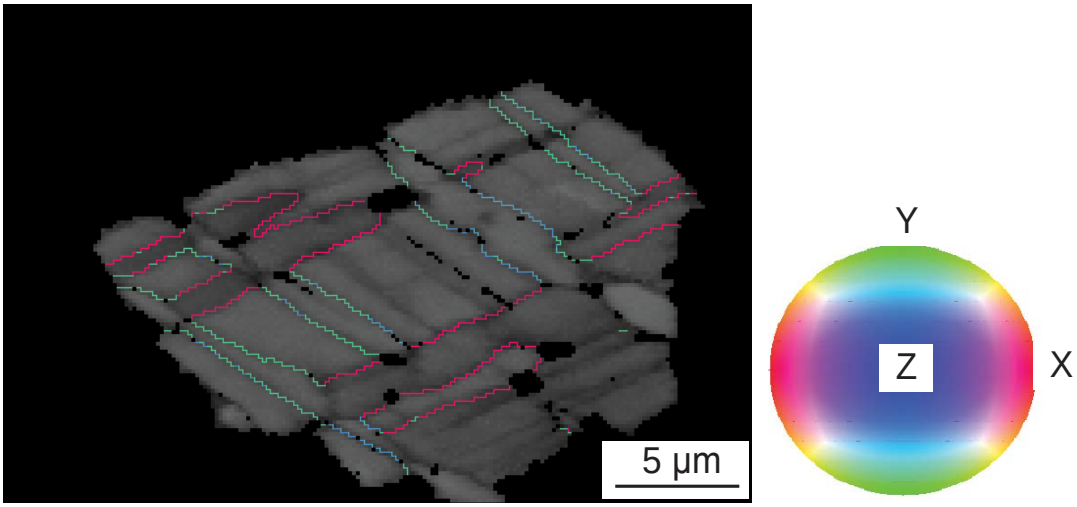

Figure S2. Band contrast map combined with misorientation axis component (in HKL Channel5 suit) of the twinned grain shown in Figure 6 in the text. The abundance of the red and green boundaries in the map indicates that there is a preferred rotation axis perpendicular to the map normal direction Z.

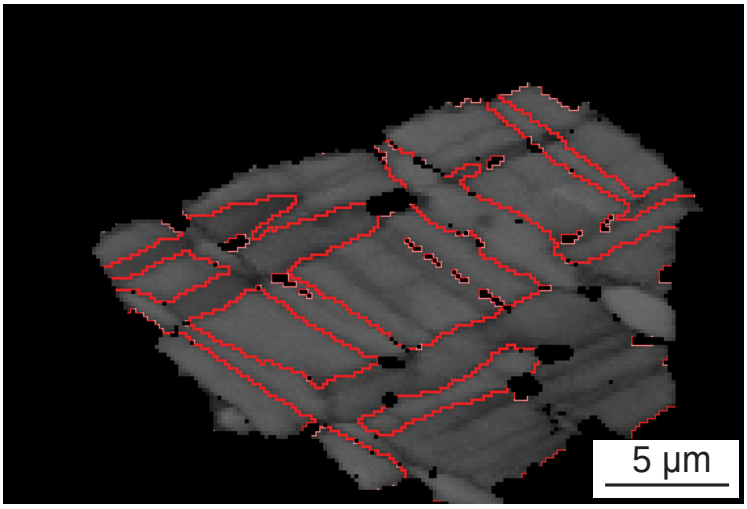

Figure S3. Band contrast map combined with special boundary component (in HKL Channel5 suit) of the twinned grain shown in Figure 6 in the text. The highlighted boundaries correspond to $\langle \mathbf{02\bar{2}1} \rangle$ misorientation axis, 85° misorientation angle, and 5° for both of the maximum deviations.

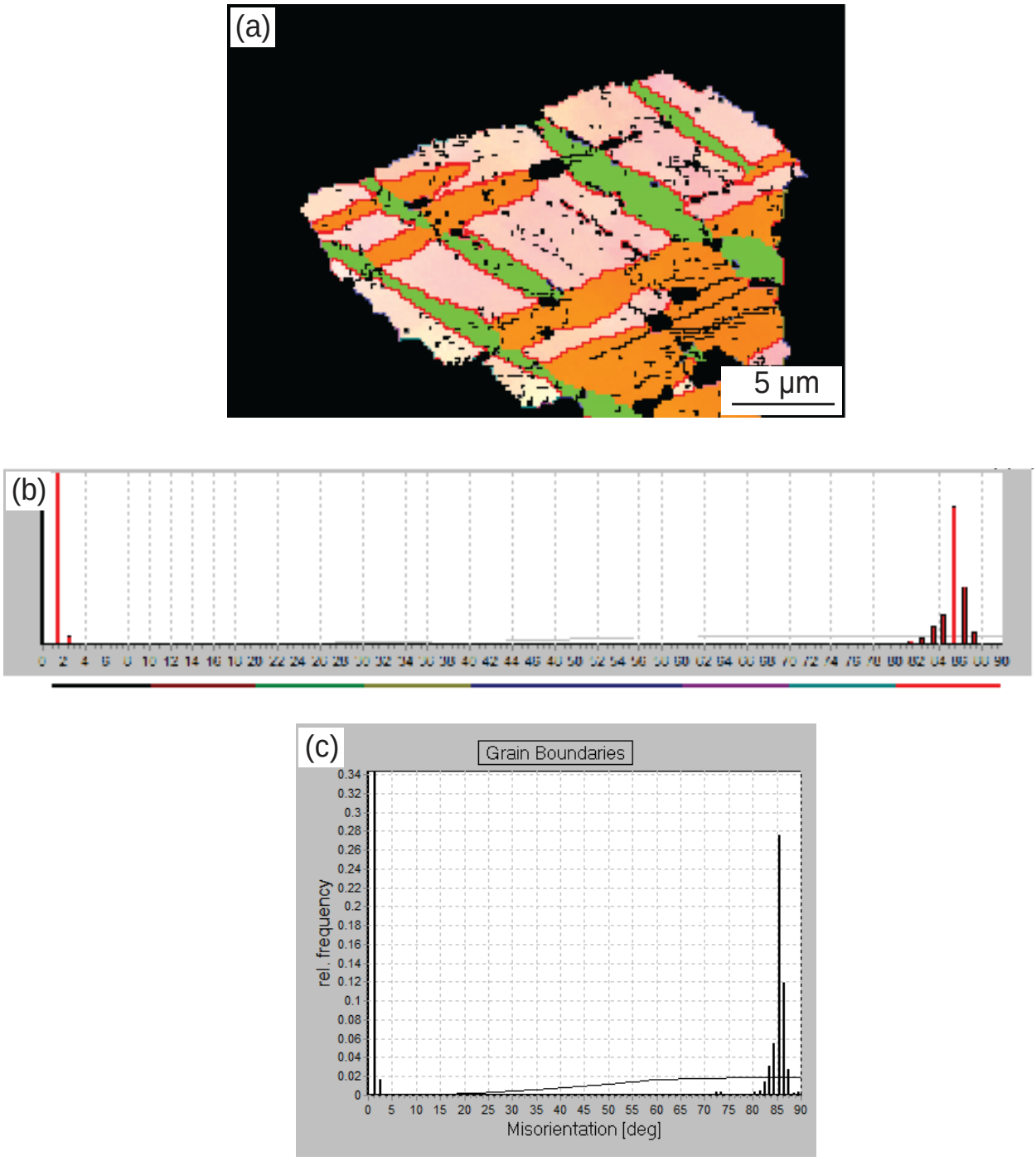

Figure S4. (a) IPF_X map combined with grain boundary component (in HKL Channel5 suit) of the twinned grain shown in Figure 6 in the text. The histograms of frequency and distribution of the boundaries are shown in (b) and (c).

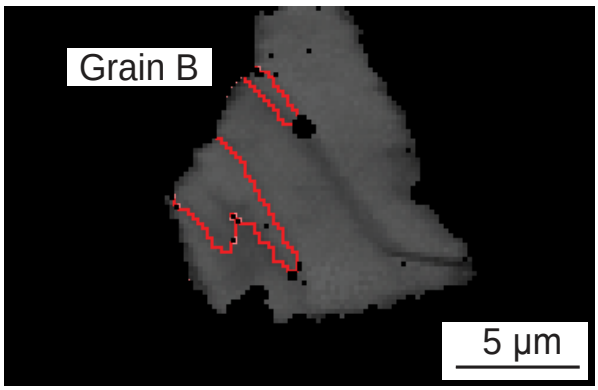

Figure S5. The band contrast map combined with special boundary component of the twinned grain C shown in Figure 11 in the text. The highlighted boundaries correspond to $\langle \mathbf{02\bar{2}1} \rangle$ misorientation axis, 85° misorientation angle, and 5° for both of the maximum deviations.

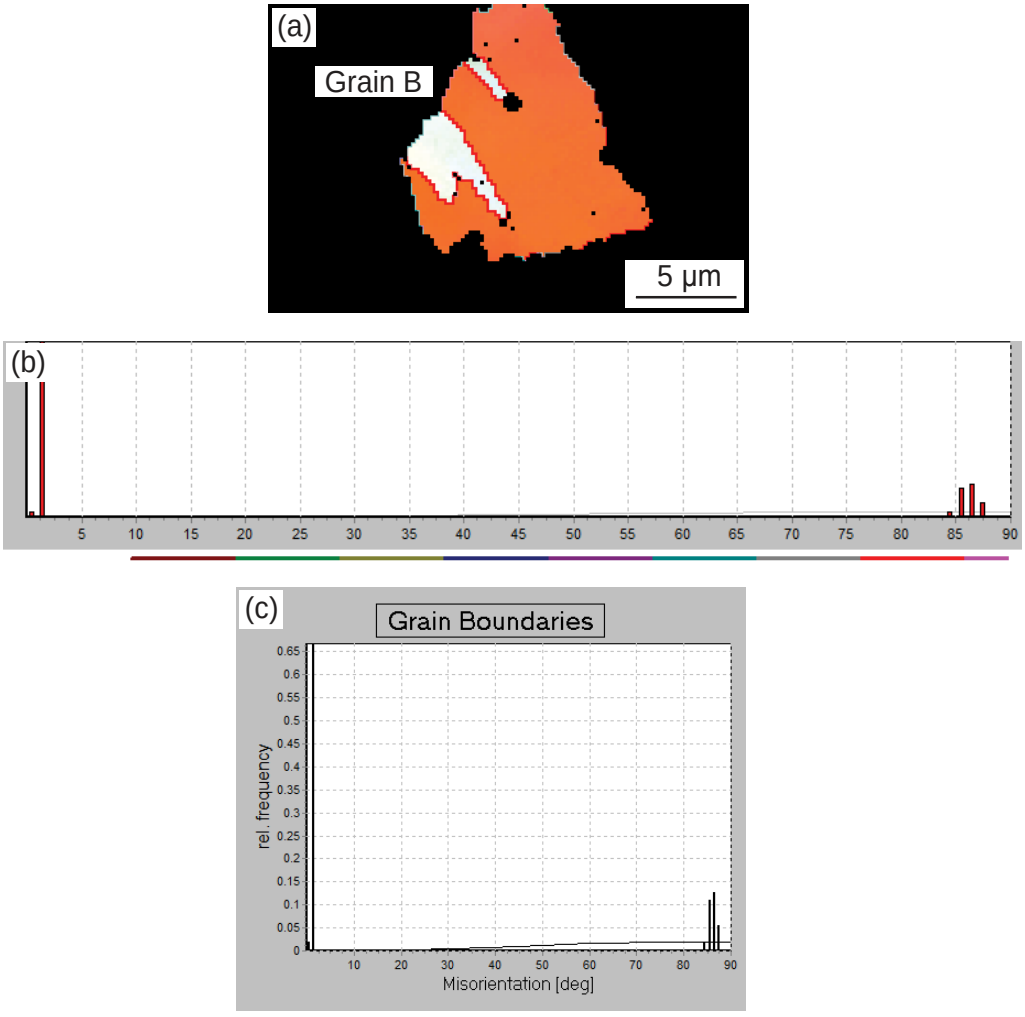

Figure S6. (a) The IPF_X map combined with grain boundary map of the twinned grain B shown in Figure 11 in the text. The histograms of frequency and distribution of the boundaries are shown in (b) and (c). Red boundaries in (a) represent the twin boundaries with 85º misorientation angle relative to the host as indicated in (b) and (c).

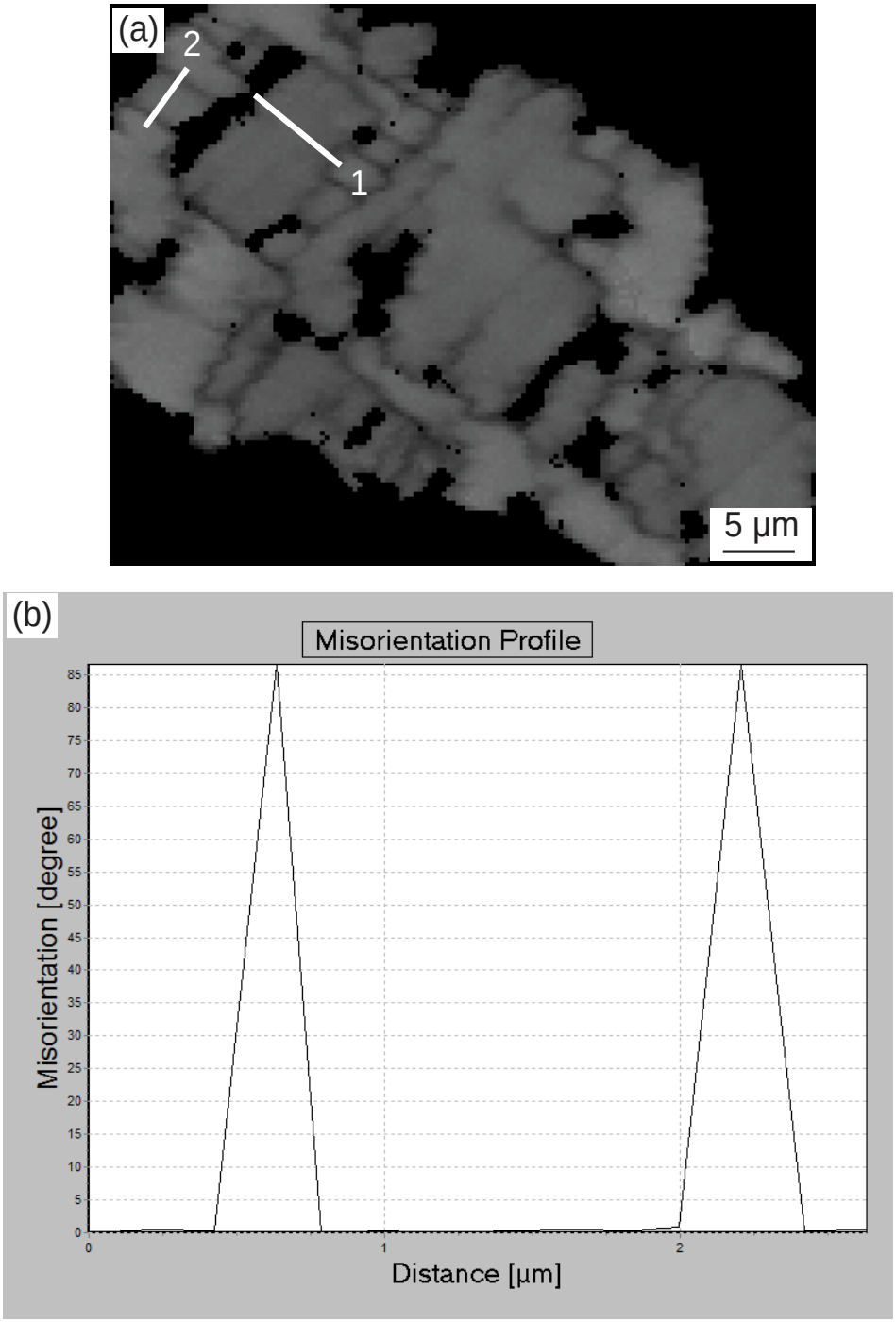

Figure S7. Results of electron backscatter diffraction (EBSD) crystal orientation mapping with a 0.15 µm step size on the twinned grain in Figure 14 in the text. (a) Band contrast map showing trace 1 across subgrain B and trace 2 across subgrain C (b) a misorientation profile along trace 1 in (a). For both twins, two peaks with misorientation angles of ~85º were measured.

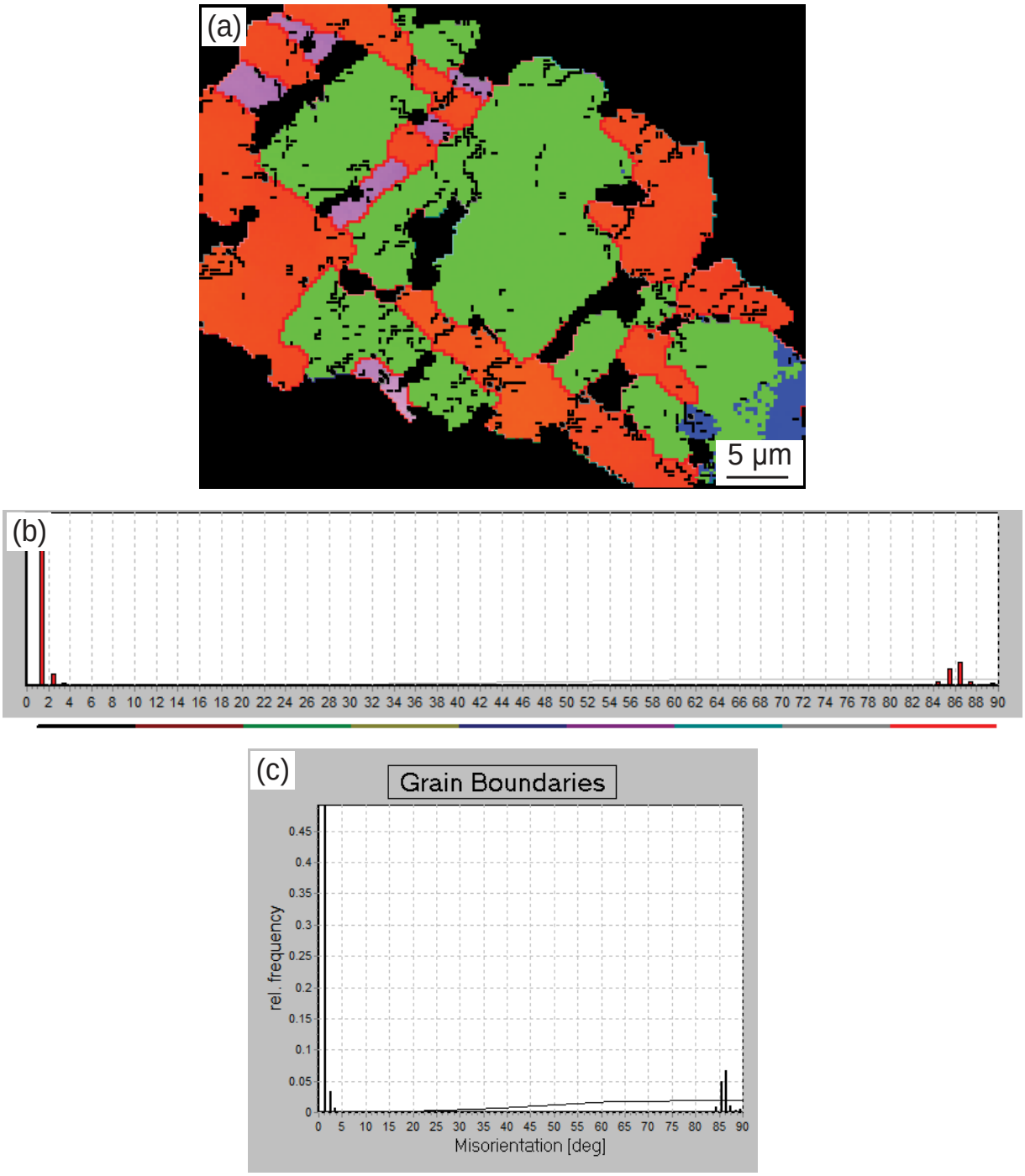

Figure S8. (a) The IPF_Z map combined with grain boundary map of the twinned grain shown in Figure 14 in the text. The histograms of frequency and distribution of the boundaries are shown in (b) and (c). Red boundaries in (a) represent the twin boundaries with 85º misorientation angle relative to the host as indicated in (b) and (c).